Inner-shell electron effects in strong-field double ionization of Xe

Zongqiang Yuan,[1,2] Difa Ye,[2] Jie Liu,[2,3,4,*] and Libin Fu[2,3,4,†]

[1]*Science and Technology on Plasma Physics Laboratory, Research Center of Laser Fusion, China Academy of Engineering Physics, Mianyang 621900, China*

[2]*National Key Laboratory of Science and Technology on Computational Physics, Institute of Applied Physics and Computational Mathematics, Beijing 100088, China*

[3]*CAPT, HEDPS, and IFSA Collaborative Innovation Center of MoE, Peking University, Beijing 100871, China*

[4]*Center for Fusion Energy Science and Technology, China Academy of Engineering Physics, Beijing 100088, China*

(Received 12 April 2016; published 8 June 2016)

We investigate theoretically the inner-shell electron effects in strong-field double ionization of Xe by a comparative study with two different three-dimensional semiclassical models, i.e., the widely used helium-like model and an improved Green–Sellin–Zachor (GSZ) model. The enhanced double-ionization signals through sequential ionization and recollision-induced excitation with subsequent field ionization are identified as two origins of the nonstructured pattern in the correlated electron momentum spectrum observed in a recent experiment [Phys. Rev. Lett. **113**, 103001 (2014)]. The relationship between these enhancements and the inner-shell electrons is revealed by back analysis of the classical trajectories.

DOI: 10.1103/PhysRevA.93.063409

I. INTRODUCTION

Atomic physics with an ultrashort intense laser field is an intriguing but challenging research area due to its nonperturbative nature (for recent reviews, see, e.g., Refs. [1–3]). Nonsequential double ionization (NSDI) of atoms in a strong laser field can trace its history back to the first observation of the knee structure on the doubly charged ionization curve of Xe atoms [4]. NSDI gains a particular significance within the strong-field community because it provides a prototype model for the study of electron-electron (e-e) correlations enforced by the external field. A substantial effort is devoted to understanding the mechanism of NSDI since the high-precision measurement of strong-field double ionization of He [5] and the recollision scenario is now broadly accepted [6]. In this mechanism, the outermost electron tunnels into the continuum through the field-suppressed Coulomb barrier and is driven back to its parent ion by the reversed electric field, delivering part of its energy to kick out another inner electron.

During the past years, the coincidence measurement of the momenta of two electrons along the laser field polarization with cold-target recoil ion momentum spectroscopy (COLTRIMS) [7] has provided a solid basis for the analysis of the underlying mechanisms of NSDI. The measurements, however, were mainly concentrated on low-Z rare-gas atoms, i.e., He, Ne, and Ar. There, one basically observed that the electrons were predominantly emitted into the same hemisphere (side-by-side emission) in the nonsequential double-ionization regime [8–12], except that back-to-back emission was surprisingly found to dominate for Ar atoms at laser intensities below the recollision threshold [13,14]. More recently, the above-mentioned dominance of side-by-side or back-to-back emissions was found to essentially disappear in a fully differential measurement on strong-field double ionization of Xe by 25 fs, 790 nm laser pulses [15]. Instead, a universal nonstructured two-electron momentum distribution emerges over a wide range of laser intensities. These new observations indicate that the current understanding of NSDI cannot be considered to be complete.

In this paper, we explore inner-shell electron effects in strong-field double ionization of Xe, following the treatment in our recent Letter [15], extending the calculations, and presenting a more detailed account of the experiments. This is facilitated by the comparative study with two different three-dimensional (3D) semiclassical models, i.e., the widely used helium-like model and an improved Green–Sellin–Zachor (GSZ) model [16]. Our calculations extend the previous simulation to an even wider range of laser intensities from 0.02 PW/cm^2 to 0.25 PW/cm^2. We find that, at the lowest and the highest intensities addressed in this paper, these two models indeed predict almost the same results. In contrast, in the intermediate-intensity regime, only calculations based on the GSZ model give rise to the nonstructured two-electron momentum spectra observed in experiment [15]. Compared with the helium-like model, the double-ionization signals through sequential ionization and recollision excitation with subsequent field ionization are strongly enhanced by as much as four orders of magnitude in the GSZ model. These enhancements are explained as a result of the inner-shell electron effects of Xe. Our study unambiguously reveals new mechanisms of strong-field double ionization of high-Z atoms.

II. METHODOLOGY

In the semiclassical approach to strong-field double ionization, the helium-like model with the two-active-electron approximation [see Fig. 1(a) for a schematic drawing of the model atom] has been routinely used and has proved to be very successful for low-Z rare-gas atoms. In this model, one electron is released at the outer edge of the field-suppressed Coulomb barrier along the field direction through quantum tunneling with a rate given by the Ammosov–Delone–Krainov (ADK) theory [17]. The tunneled electron has a Gaussian distribution on the transverse velocity and zero

*liu_jie@iapcm.ac.cn
†lbfu@iapcm.ac.cn

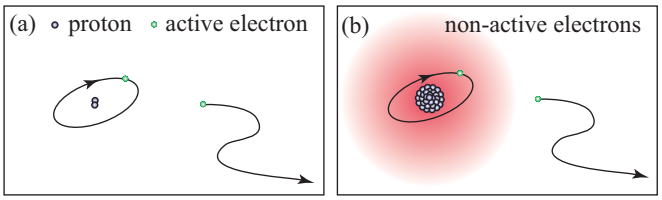

FIG. 1. Schematic drawings of model atoms. (a) In the helium-like model, there are only two protons plus two active electrons. (b) In the GSZ model, the core is constituted of Z protons and is shielded by a static electron cloud with total charge of $Z-2$.

longitudinal velocity [18–20]. The bound electron is sampled from a microcanonical distribution [21,22]. The subsequent evolution of the two electrons with the above initial conditions is governed by Newton's equations of motion: $d^2\vec{r}_i/dt^2 = -\vec{\varepsilon}(t) - \nabla_{r_i}(V^i_{ne} + V_{ee})$. Here, the index i denotes the two different electrons. $V^i_{ne} = -2/|\vec{r}_i|$ and $V_{ee} = 1/|\vec{r}_1 - \vec{r}_2|$ are Coulomb interactions between nucleus and electrons and between two electrons, respectively. The recollision-induced excitation-tunneling effect of both electrons has been included by allowing both electrons to tunnel through the potential barrier whenever they reach the outer turning point. The tunneling probability is given by the Wentzel–Kramers–Brillouin (WKB) approximation [23–25].

For high-Z atoms, to take into account of the influence of other inner-shell electrons, the above helium-like model can be improved by adopting the GSZ potential for the interaction between the core [Z protons plus $Z-2$ nonactive electrons; see Fig. 1(b)] and two active electrons $V^{\rm GSZ}_{ne}(r) = -(1/r)[2 + (Z-2)\Omega(r)]$, where $\Omega(r) = [(\eta/\xi)(e^{\xi r} - 1) + 1]^{-1}$ with the nuclear charge Z and two screening parameters η and ξ [16]. We perform three-dimensional (3D) semiclassical calculations on double ionization of Xe in a linearly polarized 800 nm laser field with both the helium-like model and the GSZ model for comparison. The atomic parameters are $Z = 54$, $\eta = 5.2075$, and $\xi = 1.1701$ for the Xe atom. The laser field $\varepsilon(t)$ has a constant amplitude for the first ten cycles and is turned off with a three-cycle ramp.

III. MAIN RESULTS

In the upper-two rows of Fig. 2, we present the correlated electron momentum spectra along the polarization direction for double ionization of Xe, calculated by the helium-like model [Figs. 2(A1)–2(A6)] and the GSZ model [Figs. 2(B1)–2(B6)], respectively. Comparing the results at the same laser intensities one by one, we find that the predictions by two models show no discernible difference at the lowest laser intensity, but differ significantly at higher intensities.

Specifically, for the helium-like model, the spectrum exhibits overall maxima in the second and forth quadrants at the lowest laser intensity [0.02 PW/cm^2, Fig. 2(A1)], indicating that two electrons are predominately emitted into the opposite hemisphere (anticorrelation). As the laser intensity increases, the spectrum presents a clear transition from anticorrelation to correlation (i.e., two electrons are predominately emitted into the same hemisphere). The dominance of the two electrons ejected via a correlated scenario nearly disappears at the highest intensity [0.25 PW/cm^2, Fig. 2(A6)]. This behavior is similar to early observations on low-Z atoms (e.g., He, Ne, and Ar) [8–14] but contradict the recent observations on Xe [15], where two-electron momentum spectra show a nonstructured

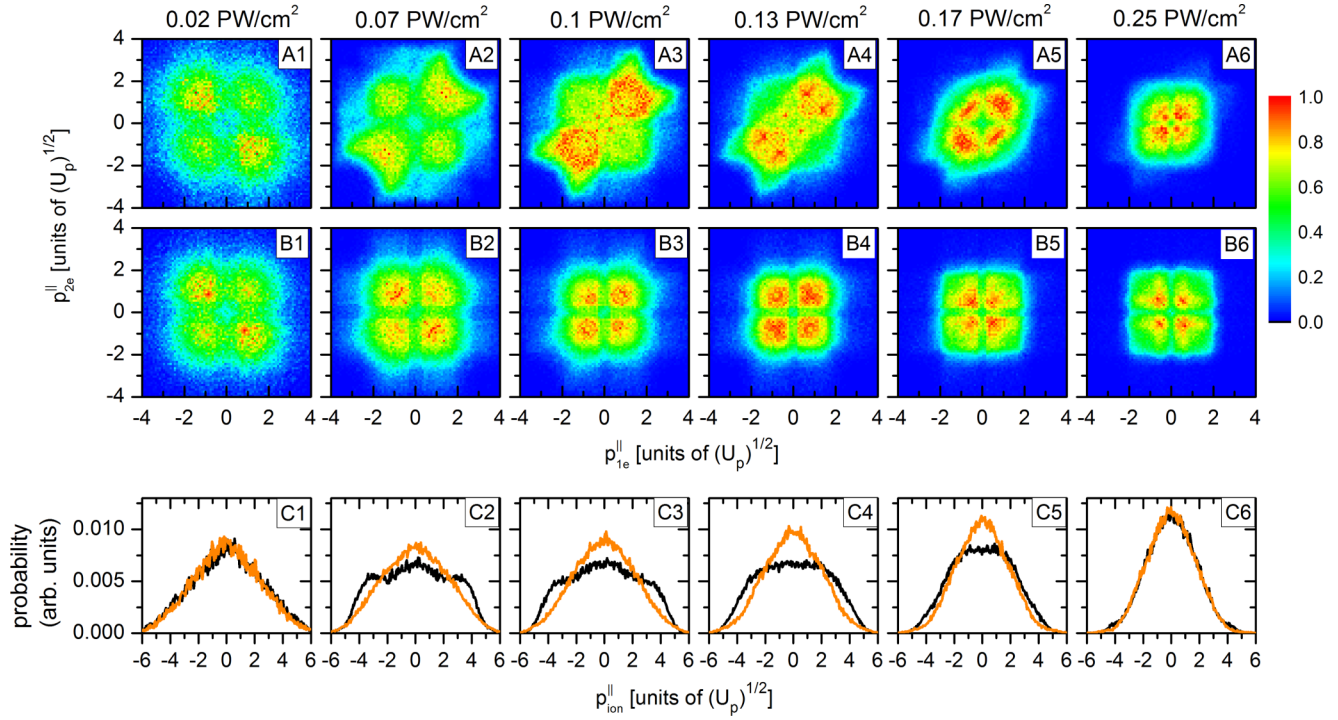

FIG. 2. Probability contour plots of correlated two-electron momentum spectrum along laser polarization calculated by (A1)–(A6) the helium-like model and (B1)–(B6) the GSZ model at intensities of 0.02–0.25 PW/cm^2. (C1)–(C6) The corresponding parallel momentum distributions of Xe^{2+} calculated by the helium-like model [black (dark gray) lines] and the GSZ model [orange (light gray) lines].

distribution over a wide range of laser intensities. This indicates that the helium-like model, although successful in explaining the general features of NSDI of low-Z atoms, fails to account for NSDI of high-Z atoms. Such discrepancies underline the quest to further extend the theory.

The *ab initio* simulation of the inner-shell electron effects, however, is currently unrealistic. The GSZ potential provides an alternative route to circumvent this problem. We recalculate the double ionization of Xe based on the GSZ model and the resulting correlated electron momentum spectra are presented in the middle row of Fig. 2. At the intensity of 0.02 PW/cm^2 [Fig. 2(B1)], a clear anticorrelated pattern is observed, which is the same as the calculation based on the helium-like model. In contrast, as the laser intensity increases, the electron correlated momenta distribute in all four quadrants almost equally. These nonstructured electron momentum spectra agree well with the experimental results. It is clear that the GSZ potential properly describes the influence of the inner-shell electrons on the double ionization of Xe.

To doubly check the validity of the improved model, we also calculate and compare the momentum distribution of Xe^{2+}, which is shown in the bottom row of Fig. 2 with black (dark gray) and orange (light gray) lines for the helium-like model and the GSZ model, respectively. The results predicted by the helium-like model exhibit a single-hump structure at the lowest intensity, converting to a platform structure as the laser intensity increases, and then again a single-hump structure at the highest intensity. Conversely, the GSZ model always predicts a single-hump structure located at the zero. We find again that the helium-like model fails to reproduce the experimental observations and the predictions of the GSZ model are entirely consistent with the experiments.

The question is, what is the physics leading to the differences between the two model predictions? In the semiclassical model, the tunneled electron is initially released at a position relatively far from the parent ion. Recollision happens only if the tunneled electron is driven back to the vicinity of the parent ion. We define $D_{\min}$ as the minimum distance between the two electrons. With this parameter we are able to identify the mechanisms of sequential double ionization (SDI) and NSDI. The distributions of $D_{\min}$ are presented in Fig. 3 for both the helium-like model [black (dark gray) lines] and the GSZ model [orange (light gray) lines] in the intensity region of 0.02–0.13 PW/cm^2.

As shown in Fig. 3(a), $D_{\min}$ exhibits a narrow distribution around 2 a.u. for both models, indicating that NSDI is the dominant mechanism for the double ionization at the intensity of 0.02 PW/cm^2. Since 0.02 PW/cm^2 is well below the recollision threshold, complicated multiple recollisions and recollision-induced excitation tunneling are responsible for the anticorrelated pattern observed in Figs. 2(A1) and 2(B1) [14,25,26]. As the intensity increases, the distribution of $D_{\min}$ calculated by the helium-like model experiences no qualitative change, while for the GSZ model a broad hump structure extending up to 8 a.u. emerges at intensities above 0.1 PW/cm^2 [orange (light gray) lines in Figs. 3(c) and 3(d)]. The substantial extension of the distribution of $D_{\min}$ is a signal of the emergence of SDI. Based on these calculations, we claim that the dominance of SDI over NSDI is the mechanism for

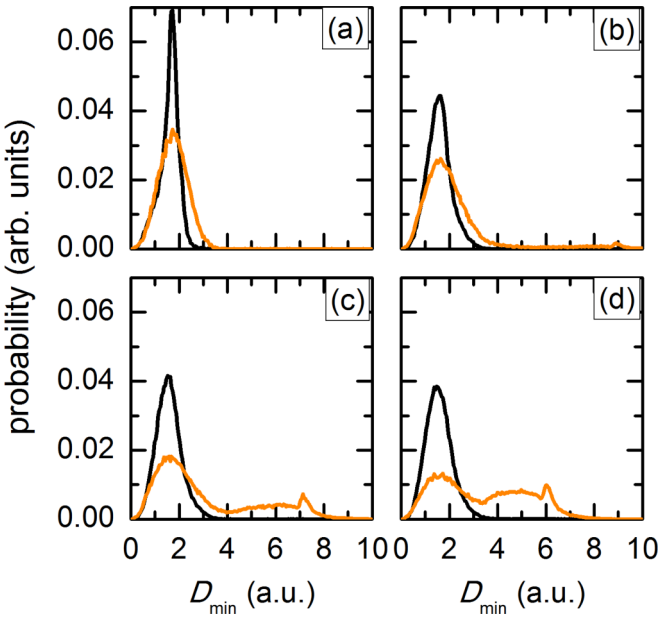

FIG. 3. Probability distributions of the minimum distance between two electrons for both the helium-like model [black (dark gray) lines] and the GSZ model [orange (light gray) lines] at intensities of (a) 0.02, (b) 0.07, (c) 0.1, and (d) 0.13 PW/cm^2.

the nonstructured momentum spectra of the double ionization of Xe at high intensities above 0.1 PW/cm^2.

The SDI signal, however, is very weak at a slightly lower laser intensity [e.g., 0.07 PW/cm^2, orange (light gray) line in Fig. 3(b)]. This cannot explain why the correlated electron momentum spectrum also shows a nonstructured distribution [Fig. 2(B2)], pointing to the existence of another mechanism. We further classify the NSDI trajectories into two categories, the recollision-induced direct ionization (RIDI) and the recollision excitation with subsequent field ionization (RESI) [25]. The former typically results in same-hemisphere emission right after the recollision, while the latter also leads to opposite-hemisphere emission. To identify these two different processes, we analyze the differential ionization yield in the (θ,t_d) plane. Here, $\theta = \arctan(p_{2e}^{\parallel}/p_{1e}^{\parallel})$ is an indicator of the correlation between two electrons' momentum [27,28]. We restrict θ to be in the domain $[0,2\pi]$. Thus $\theta \in [0,\pi/2]$ and $[\pi,3\pi/2]$ correspond to same-hemisphere emissions while $\theta \in [\pi/2,\pi]$ and $[3\pi/2,2\pi]$ correspond to opposite-hemisphere emissions. t_d is the time delay between recollision and double ionization with the double-ionization time defined as the instant when the energy of either electron becomes positive and never returns to negative. A time delay within a half laser cycle is the signal of the RIDI pathway, while the rest corresponds to the RESI pathway.

Figure 4 presents the differential ionization yield in the (θ,t_d) plane at the intensity of 0.07 PW/cm^2. The results indicate that the RESI pathway substantially increases and dominates over the RIDI pathway in the GSZ model as compared with the helium-like model. Since the RESI pathway results in equal same-hemisphere emission and opposite-hemisphere emission of the two electrons, this gives rise to

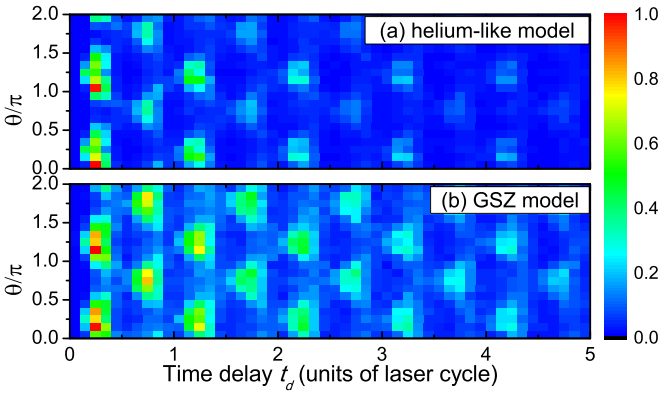

FIG. 4. Differential ionization yield over the phase angle θ and the time delay t_d, calculated by (a) the helium-like model and (b) the GSZ model, respectively (see text for detail). The laser intensity is 0.07 PW/cm^2.

the second origin of the observed nonstructured pattern on the correlated electron momentum spectra.

Based on the proceeding discussions, we conclude that the nonstructured momentum spectra is closely related to the abundance of SDI and RESI at the high and intermediate laser intensities, respectively. Both mechanisms have the same feature that somewhat involves the field-assisted tunneling ionization or over-the-barrier ionization of the singly charged ion as the final step of the double-ionization process. Thus they are sensitive to the slight change of the electronic structure because the ionization rate exponentially depends on the area of the Coulomb barrier.

Quantitative verification of this picture is shown in Fig. 5. Here we first present the radial distribution of the bound electron without the laser field in Fig. 5(a). It can be seen that the electron in the GSZ model has a broader distribution and thus is closer to the exit of the barrier and easier to be ionized by the laser field as compared with that in the helium-like model. The same conclusion can be drawn by analyzing the structure of the Coulomb barrier shown in Figs. 5(c) and 5(d), where the Coulomb barrier in the GSZ model [orange (light gray) lines] is slightly narrower than that in the helium-like model [black (dark gray) lines]. One should note, however, that such minor difference leads to dramatically increased number of field-assisted ionization events in the GSZ-model predictions, up to four orders of magnitude as far as we can see in Figs. 5(b) at 0.1 PW/cm^2. This explains why we find a long tail in the distributions of $D_{\min}$ for the GSZ model [orange (light gray) lines in Figs. 3(c) and 3(d)] but not for the helium-like model [black (dark gray) lines]. It is also the reason for the dominance of double-ionization events with long time delay in Fig. 4(b). The hatched area shrinks from Fig. 5(c) to Fig. 5(d), indicating that the difference between the two model predictions decreases with increasing laser intensity. As

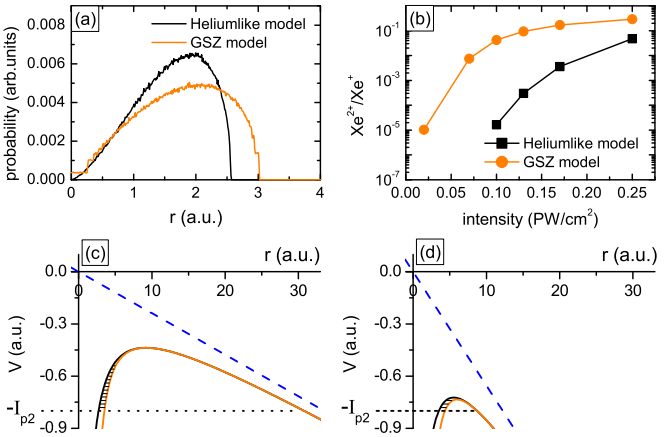

FIG. 5. (a) Radial distribution of bound electron of Xe^+ without laser field. (b) Ionization probability of Xe^+ as a function of laser intensity. The simulation starts from a microcanonical ensemble of Xe^+ ion with the single-active-electron approximation. (c) Sketch of the atomic potentials suppressed by the laser field, with the black (dark gray) and orange (light gray) curves for the helium-like model and GSZ model, respectively. Panel (d) is the same as panel (c) but at a higher laser intensity.

a result, both the momentum spectra of the correlated electrons and the doubly charged ion calculated by the two models seem roughly the same at the highest laser intensity in Fig. 2.

IV. CONCLUSION

In summary, we studied and disentangled the mechanisms behind the strong-field double ionization of high-Z atoms. Due to the increased number of inner-shell electrons, the interaction between the nuclei and the two active electrons significantly deviates from the standard form of Coulomb potential, which results in the shrink of the potential barrier, leading to the dramatic increase of the SDI events in the high-intensity regime and the increase of the RESI events in the intermediate-intensity regime. Both mechanisms lead to nonstructured correlated electron momentum spectrum and the Gaussian distribution in the momentum spectrum of the doubly charged ion. This ultimately explains the recent experiment on Xe in nice detail.

ACKNOWLEDGMENTS

This work is supported by the National Basic Research Program of China (973 Program) (Grants No. 2013CBA01502 and No. 2013CB834100), the National Natural Science Foundation of China (Grants No. 11374040, No. 11274051, No. 11304018, and No. 11475027), the Foundation of President of the China Academy of Engineering Physics (Grant No. 2014-1-029), and the CAEP-FESTC (Grant No. J2014-0401-03).

[1] P. B. Corkum, Phys. Today **64**, 36 (2011).
[2] W. Becker, X. Liu, P. J. Ho, and J. H. Eberly, Rev. Mod. Phys. **84**, 1011 (2012).
[3] Liang-You Peng, Wei-Chao Jiang, Ji-Wei Geng, Wei-Hao Xiong, and Qihuang Gong, Phys. Rep. **575**, 1 (2015).

[4] A. l'Huillier, L. A. Lompre, G. Mainfray, and C. Manus, Phys. Rev. A **27**, 2503 (1983).
[5] B. Walker, B. Sheehy, L. F. DiMauro, P. Agostini, K. J. Schafer, and K. C. Kulander, Phys. Rev. Lett. **73**, 1227 (1994).
[6] P. B. Corkum, Phys. Rev. Lett. **71**, 1994 (1993).
[7] R. Dörner, V. Mergel, O. Jagutzki, L. Spielberger, J. Ullrich, R. Moshammer, and H. Schmidt-Böcking, Phys. Rep. **330**, 95 (2000).
[8] Th. Weber, H. Giessen, M. Weckenbrock, G. Urbasch, A. Staudte, L. Spielberger, O. Jagutzki, V. Mergel, M. Vollmer, and R. Dörner, Nature (London) **405**, 658 (2000).
[9] B. Feuerstein, R. Moshammer, D. Fischer *et al.*, Phys. Rev. Lett. **87**, 043003 (2001).
[10] M. Weckenbrock, D. Zeidler, A. Staudte *et al.*, Phys. Rev. Lett. **92**, 213002 (2004).
[11] A. Staudte, C. Ruiz, M. Schöffler *et al.*, Phys. Rev. Lett. **99**, 263002 (2007).
[12] A. Rudenko, V. L. B. de Jesus, T. Ergler, K. Zrost, B. Feuerstein, C. D. Schröter, R. Moshammer, and J. Ullrich, Phys. Rev. Lett. **99**, 263003 (2007).
[13] Yunquan Liu, S. Tschuch, A. Rudenko, M. Dürr, M. Siegel, U. Morgner, R. Moshammer, and J. Ullrich, Phys. Rev. Lett. **101**, 053001 (2008).
[14] Yunquan Liu, Difa Ye, Jie Liu, A. Rudenko, S. Tschuch, M. Dürr, M. Siegel, U. Morgner, Qihuang Gong, R. Moshammer, and J. Ullrich, Phys. Rev. Lett. **104**, 173002 (2010).
[15] Xufei Sun, Min Li, and Difa Ye *et al.*, Phys. Rev. Lett. **113**, 103001 (2014).
[16] A. E. S. Green, D. L. Sellin, and A. S. Zachor, Phys. Rev. **184**, 1 (1969); P. P. Szydlik and A. E. S. Green, Phys. Rev. A **9**, 1885 (1974); R. H. Garvey, C. H. Jackman, and A. E. S. Green, *ibid.* **12**, 1144 (1975).
[17] M. V. Ammosov, N. B. Delone, and V. P. Krainov, Zh. Eksp. Teor. Fiz. **91**, 2008 (1986) [Sov. Phys. JETP **64**, 1191 (1986)].
[18] J. Chen, J. Liu, L. B. Fu, and W. M. Zheng, Phys. Rev. A **63**, 011404(R) (2000).
[19] L.-B. Fu, J. Liu, J. Chen, and S.-G. Chen, Phys. Rev. A **63**, 043416 (2001).
[20] L.-B. Fu, J. Liu, and S.-G. Chen, Phys. Rev. A **65**, 021406(R) (2002).
[21] J. G. Leopold and I. C. Percival, J. Phys. B: At. Mol. Phys. **12**, 709 (1979).
[22] C. O. Reinhold and C. A. Falcón, Phys. Rev. A **33**, 3859 (1986).
[23] J. S. Cohen, Phys. Rev. A **64**, 043412 (2001).
[24] K. I. Dimitriou, D. G. Arbó, S. Yoshida, E. Persson, and J. Burgdörfer, Phys. Rev. A **70**, 061401 (2004).
[25] D. F. Ye and J. Liu, Phys. Rev. A **81**, 043402 (2010).
[26] S. L. Haan, Z. S. Smith, K. N. Shomsky, and P. W. Plantinga, J. Phys. B: At., Mol. Opt. Phys. **41**, 211002 (2008).
[27] J. Liu, D. F. Ye, J. Chen, and X. Liu, Phys. Rev. Lett. **99**, 013003 (2007).
[28] D. F. Ye, J. Chen, and J. Liu, Phys. Rev. A **77**, 013403 (2008).